magnetochemistry

MDPI

Article

An Organic–Inorganic Hybrid Semiconducting Quantum Spin Liquid Candidate: (BEDT-TTF)$_3$[Cu$_2$(μ-C$_2$O$_4$)$_3$·CH$_3$CH$_2$OH·1.2H$_2$O]

Bin Zhang [1,*,†], Yan Zhang [2,*,†], Dongwei Wang [3], Zheming Wang [4,*], Guangcai Chang [5], Zengqiang Gao [5], Yanjun Guo [3], Fen Liu [6], Zhijuan Zhao [6], Xiaoyu Zhang [6], Baolong Qu [6], Peng Xu [3], Jiaou Wang [5], Fenliang Dong [3], Tongling Liang [6], Yang Sun [6], Deliang Yang [6], Qiaolian Li [6], Xiaofei Luo [6], Rongjuan Feng [6], Mei Liu [6] and Xueying Zhang [6]

1 Organic Solid Laboratory, BNLMS, CMS & Institute of Chemistry, Chinese Academy of Sciences, Beijing 100190, China
2 Institute of Condensed Matter and Material Physics, School of Physics, Peking University, Beijing 100871, China
3 CAS Key Laboratory of Standardization and Measurement for Nanotechnology, National Center for Nanoscience and Technology, Beijing 100190, China
4 State Key Laboratory of Rare Earth Materials Chemistry and Applications, BNLMS, College of Chemistry and Molecular Engineering, Peking University, Beijing 100871, China
5 BSRF, Institute of High Energy Physics, Chinese Academy of Sciences, Beijing 100047, China
6 Institute of Chemistry, Chinese Academy of Sciences, Beijing 100190, China
* Correspondence: zhangbin@iccas.ac.cn (B.Z.); zhang_yan@pku.edu.cn (Y.Z.); zmw@pku.edu.cn (Z.W.)
† These authors contributed equally to this work.

Abstract: The organic–inorganic hybrid (BEDT-TTF)$_3$[Cu$_2$(μ-C$_2$O$_4$)$_3$·CH$_3$CH$_2$OH·1.2H$_2$O] (**I**) was obtained using the electrocrystallization method. It comprises a θ^{21}-phase organic donor layer and a two-dimensional inorganic antiferromagnetic honeycomb lattice. Cu(II) is octahedrally coordinated by three bisbidenetate oxalates, exhibiting Jahn–Teller distortion. CH$_3$CH$_2$OH and H$_2$O molecules are located within the cavities of the honeycomb lattice. The total formal charge of the three donor molecules was assigned to be +2 based on the bond lengths in the TTF core, which corresponded to the Raman spectra. It is a semiconductor with σ_{rt} = 0.04 S/cm and E_α = 40 meV. No long-range ordering was observed above 2 K from zero-field cooling/field cooling magnetization, as confirmed by specific heat measurements. The spin frustration with f > 10 from the antiferromagnetic copper-oxalate-framework was observed. It is a candidate quantum spin liquid.

Keywords: Jahn–Teller effect; Cu(II); oxalate; single crystal; conductivity; spin frustration; quantum spin liquid candidate

check for updates

Academic Editor: You Song

Received: 25 November 2024
Revised: 21 January 2025
Accepted: 10 February 2025
Published: 12 February 2025

Citation: Zhang, B.; Zhang, Y.; Wang, D.; Wang, Z.; Chang, G.; Gao, Z.; Guo, Y.; Liu, F.; Zhao, Z.; Zhang, X.; et al. An Organic–Inorganic Hybrid Semiconducting Quantum Spin Liquid Candidate: (BEDT-TTF)$_3$[Cu$_2$(μ-C$_2$O$_4$)$_3$·CH$_3$CH$_2$OH·1.2H$_2$O]. *Magnetochemistry* **2025**, *11*, 12. https://doi.org/10.3390/magnetochemistry11020012

Copyright: © 2025 by the authors. Licensee MDPI, Basel, Switzerland. This article is an open access article distributed under the terms and conditions of the Creative Commons Attribution (CC BY) license (https://creativecommons.org/licenses/by/4.0/).

1. Introduction

In 1973, P. W. Anderson proposed that in a S = 1/2 antiferromagnetic interaction triangular lattice, magnetic ordering or freezing is not observed due to spin frustration, resulting in a quantum spin liquid [1]. In 1987, he suggested that the insulating antiferromagnet La$_2$CuO$_4$ acts as the parent compound of the cuprate superconductor after hole doping [2,3]. Quantum spin liquids with two-dimensional lattices, including triangular lattices, Kagome lattices and honeycomb lattices, have been proposed [4,5]. Quantum spin liquids have emerged as a central focus in condensed matter physics due to their strong connection to magnetism and conductivity. Numerous molecular superconductors have been identified within hybrid organic–inorganic charge–transfer complexes [6]. These complexes also provide strong support for research into quantum spin liquid candidates. The behavior of quantum spin liquids was identified in organic–inorganic hybrid charge–transfer complexes,

such as κ-(BEDT-TTF)$_2$[Cu$_2$(CN)$_3$] (BEDT-TTF = bis(ethylenedithio)tetrathiafulvalene), κ-(BEDT-TTF)$_2$[Ag$_2$(CN)$_3$], EtMe$_3$Sb[Pd(dmit)$_2$]$_2$ (dmit = 1,3-dithiol-2-thione-4,5-dithiolate) and κ-H$_3$(cat-EDT-TTF)$_2$. κ-(BEDT-TTF)$_2$[Cu$_2$(CN)$_3$] features a triangular lattice, while (EDT-TTF-CONH$_2$)$_6$[Re$_6$Se$_8$(CN)$_6$] exhibits a Kagome lattice [7–11].

Oxalate ($C_2O_4^{2-}$), one of the most commonly used short connectors, plays a crucial role in molecular superconductors, molecular conductors and molecular magnets. The exchange coupling in oxalate-bridged binuclear Cu(II) has been extensively studied [12]. Long-range ordering has been reported in metal–oxalate frameworks, ranging from one-dimensional chains such as K$_2$[Fe(μ-C$_2$O$_4$)(C$_2$O$_4$)], A[Fe(μ-C$_2$O$_4$)Cl$_2$] (A = alkyl ammonium), K$_2$[Co(μ-C$_2$O$_4$)(C$_2$O$_4$)] and [Co(μ-C$_2$O$_4$)(μ-HOC$_3$H$_6$OH)] to two-dimensional layers like [(C$_4$H$_9$)$_4$N][MCr(μ-C$_2$O$_4$)$_3$] (M = Mn^{2+}, Fe^{2+}, Co^{2+}, Ni^{2+}, Cu^{2+}, Zn^{2+}), A[$M^{II}Fe^{III}$(μ-C$_2$O$_4$)$_3$] (A = ammonium; M = Mn, Fe), [Fe(μ-C$_2$O$_4$)(μ-CH$_3$OH)] and [Fe$_2$(μ-C$_2$O$_4$)$_3$]·4H$_2$O, and extending to three-dimensional metal–oxalate networks such as, [Zn^{II}(bpy)$_3$][$M^{II}Cr^{III}$(μ-C$_2$O$_4$)$_3$][ClO$_4$] (Z = Mn, Fe, Co, Ni; M = Mn, Fe, Co, Ni, Cu, Zn), [Co(bpy)$_3$][Co$_2$(μ-C$_2$O$_4$)$_3$]ClO$_4$, [(Me$_4$N)$_6$[Mn$_3$Cr$_4$(μ-C$_2$O$_4$)$_{12}$]·6H$_2$O and [Mn(μ-C$_2$O$_4$)]·0.25H$_2$O. Additionally, a single-chain magnet, [C$_{12}$H$_{24}$O$_6$K]$_{0.5}$[(C$_{12}$H$_{24}$O$_6$)(FC$_6$H$_4$NH$_3$)]$_{0.5}$[Co(H$_2$O)$_2$Cr(μ-C$_2$O$_4$)$_2$(C$_2$O$_4$)], has been reported [13–26].

The magnetism and conductivity of M(C$_2$O$_4$)$_2^{2-}$, characterized by a square anion, have been investigated. A molecular conductor with a room-temperature conductivity of 320 S/cm was observed in Mg$_{0.33}$[Pt(C$_2$O$_4$)$_2$]·5.3H$_2$O. It exhibits a metal-to-insulator transition alongside a spin–Peierls transition [27,28]. When the metal cation was replaced with an organic donor, the paramagnetic conductors (BEDT-TTF)$_2$[Pt(C$_2$O$_4$)$_2$] and (BEDT-TTF)$_2$[Cu(C$_2$O$_4$)$_2$] were obtained, and a metal–insulator transition took place at 65 K [29–31].

The magnetism and conductivity of organic–inorganic hybrid charge–transfer complexes composed of an organic donor and M(C$_2$O$_4$)$_3^{3-}$, featuring an octahedral anion, were also examined. The first paramagnetic superconductor containing a paramagnetic metal ion, β″-(BEDT-TTF)$_3$[Fe(C$_2$O$_4$)$_3$(H$_3$O)·C$_6$H$_5$CN], along with the semiconductor paramagnets β″-(BEDT-TTF)$_3$[KFe(C$_2$O$_4$)$_3$·C$_6$H$_5$CN] and β″-(BEDT-TTF)$_3$[(NH$_4$)Fe(C$_2$O$_4$)$_3$·C$_6$H$_5$CN], were synthesized [32,33]. The insulating TTF$_2$[Fe(μ-C$_2$O$_4$)Cl$_2$], (BEDT-TTF)[Fe(C$_2$O$_4$)Cl$_2$]·CH$_2$Cl$_2$, semiconductive [BEDT-TTF]$_2$[Fe(μ-C$_2$O$_4$)Cl$_2$] and metallic β-BETS$_2$[Fe(μ-C$_2$O$_4$)Cl$_2$] (BETS = bis(ethylenedithio)tetraselenafulvalene) antiferromagnet were derived from a one-dimensional [Fe(μ-C$_2$O$_4$)Cl$_2^-$]$_n$ zigzag chain. A π–d interaction between the donor and the anion was observed [14,34–37]. The metallic ferromagnets β-(BEDT-TTF)$_3$[CrMn(μ-C$_2$O$_4$)$_3$] and β-BETS$_3$[CrMn(μ-C$_2$O$_4$)$_3$]·CH$_2$Cl$_2$ were derived from an oxalate-bridged two-dimensional [CrMn(μ-C$_2$O$_4$)$_3$] anion, which formed a honeycomb lattice. Their magnetic behavior is identical to that of [(C$_4$H$_9$)$_4$N][CrMn(μ-C$_2$O$_4$)$_3$] [18,38–40].

The Jahn–Teller effect on the charge–transfer complexes within copper–oxalate frameworks has previously been studied [41]. The ferromagnetic insulator [(CH$_3$)$_3$NH]$_2$[Cu(μ-C$_2$O$_4$)(C$_2$O$_4$)]·2.5H$_2$O and weak ferromagnetic insulator [(C$_2$H$_5$)$_3$NH]$_2$[Cu(μ-C$_2$O$_4$)(C$_2$O$_4$)]·H$_2$O, derived from the one-dimensional zigzag chain [Cu(μ-C$_2$O$_4$)(C$_2$O$_4$)$^{2-}$], were obtained and characterized [42]. Spin frustration with [Cu$_2$(μ-C$_2$O$_4$)$_3^{2-}$], which has a honeycomb lattice, as the quantum spin liquid candidate was discovered in organic–inorganic hybrid charge–transfer complexes, including the insulator [(C$_3$H$_7$)$_3$NH]$_2$[Cu$_2$(μ-C$_2$O$_4$)$_3$·2.2H$_2$O], the semiconductor θ^{21}-(BEDT-TTF)$_3$[Cu$_2$(μ-C$_2$O$_4$)$_3$·2CH$_3$OH] and the conductor θ^{21}-BETS$_3$[Cu$_2$(μ-C$_2$O$_4$)$_3$·2CH$_3$OH] [43–45]. A quantum spin liquid candidate from a three-dimensional copper-oxalate-framework with a hyperhoneycomb lattice was studied [46,47]. Further research on the role of the Jahn–Teller effect in organic–inorganic hybrids containing a copper–oxalate framework will help identify molecular conductors/superconductors and quantum spin liquid candidates. A new hybrid organic–

inorganic change–transfer complex, θ^{21}-(BEDT-TTF)$_3$[Cu$_2$(μ-C$_2$O$_4$)$_3$·C$_2$H$_5$OH·1.2H$_2$O] (**I**), was obtained, and related work is presented here.

2. Experiment and Discussion

BEDT-TTF was acquired from the TCI company (Tokyo, Japan). [(C$_2$H$_5$)$_3$NH]$_2$Cu$_2$(μ-C$_2$O$_4$)$_3$ was synthesized from Cu(NO$_3$)$_2$·6H$_2$O, and H$_2$C$_2$O$_4$·2H$_2$O and (C$_2$H$_5$)$_3$N were synthesized from CH$_3$OH, which was confirmed through elemental analysis, IR spectra and powder X-ray diffraction [46]. A total of 5.0 mg of BEDT-TTF and 30.0 mg of [(C$_2$H$_5$)$_3$NH]$_2$Cu$_2$(μ-C$_2$O$_4$)$_3$ were dissolved in a mixture of 25.0 mL of distilled C$_6$H$_5$Cl and 5.0 mL of distilled C$_2$H$_5$OH, and the mixture was then placed in an electrocrystallization cell. The cell was subjected to a constant source of 0.20 mA at room temperature. Shiny black, thin-plate crystals of compound (**I**) were obtained on the cathode after two weeks. The single crystals, with fresh crystal surface cleavage carried out using scotch tape, were utilized for EDS and XPS experiments [48]. The element analysis carried out using EDS revealed a composition ratio of S:Cu = 12:1, indicating a donor-to-Cu ratio of 3:2. The characteristic photoelectron peaks of Cu2p, S2p, O1S and C1S were detected in the XPS spectra.

A piece of the single crystal was selected for use in single-crystal X-ray diffraction experiments at the Beijing Radiation Synchrony Facility using λ = 0.70 Å at 290 K, a Rigaku SuperNova diffractometer with Mo radiation (λ = 0.71073 Å) at 290 K, 180 K and 120 K and a Rigaku XtalAB synergy R, HyPix diffractometer with Cu (λ = 1.54184 Å) at 100 K. The crystal structure was solved using the direct method and refined with the full-matrix least-square of F^2 using the SHELXL program [49]. The non-hydrogen atoms on BEDT-TTF, Cu, oxalate were refined anisotropically. The hydrogen atoms on BEDT-TTF were located through calculation, and refined isotropically. The solvent molecules present in the cavity were defined by the solvent MASK program. The crystals from different cells were subjected to a single-crystal X-ray diffraction experiment. The crystal structure remained the same. The compound remained stable from 290 K to 100 K. The crystallographic data from the experiments carried out at 290 K, 180 K and 120 K are listed in Table S1. The following discussion refers to the data from the experiment carried out at 100 K.

Compound **I** crystallizes in a triclinic system with the following cell parameters: a = 8.6724(2) Å; b = 16.7949(6) Å; c = 19.5607 Å; α = 74.096(3)°; β = 89.296(2)°; γ = 88.086(2)°; V = 2738.5(1) Å^3; and Z = 2, $P\bar{1}$ at 100 K. There are 2 full and 2 half BEDT-TTF molecules, 2 Cu, 3 oxalates, 2 half ethanol molecules, 0.7 H$_2$O and 0.5 H$_2$O in an independent unit (Figure 1). This is different from θ^{21}-(BEDT-TTF)$_3$[Cu$_2$(μ-C$_2$O$_4$)$_3$·2CH$_3$OH] and θ^{21}-(BETS-TTF)$_3$[Cu$_2$(μ-C$_2$O$_4$)$_3$·2CH$_3$OH], which have three donor molecules, two Cu, three oxalates and two methanol molecules which coexist in an independent unit.

The donor molecules are stacked face-to-face along the a axis to create a donor column. Donor columns are arranged side-by-side along the b axis to form a donor layer in the form of a θ^{21}-phase, which is observed in θ^{21}-(BEDT-TTF)$_3$[Cu$_2$(μ-C$_2$O$_4$)$_3$·2CH$_3$OH] and θ^{21}-(BETS-TTF)$_3$[Cu$_2$(μ-C$_2$O$_4$)$_3$·2CH$_3$OH] (Figure 2) [44,45]. One of the ethylene groups on BEDT-TTF is disordered at 290 K and ordered below 180 K. This is similar to [(C$_2$H$_5$)$_3$NH]$_2$[Cu$_2$(μ-C$_2$O$_4$)$_3$], which exhibits a disorder-to-order transition of its ethylene group at 170 K [46]. There are also S···S contacts between donor molecules.

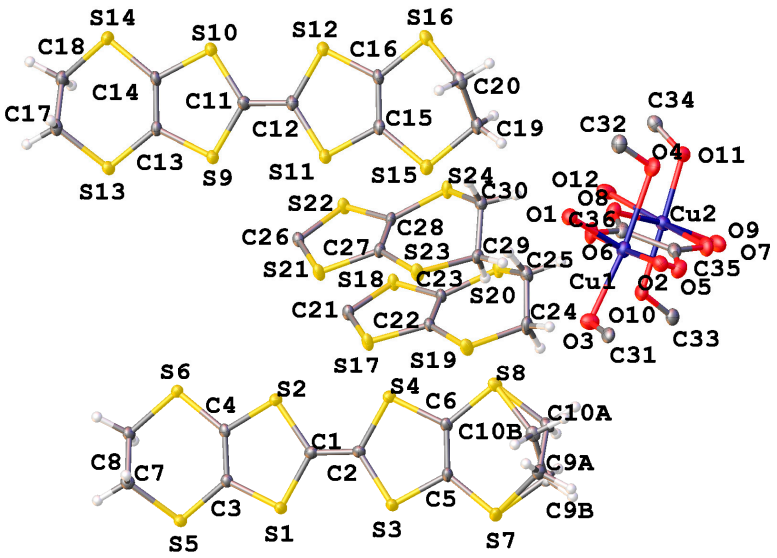


Figure 1. Atoms in an independent unit of **I**.

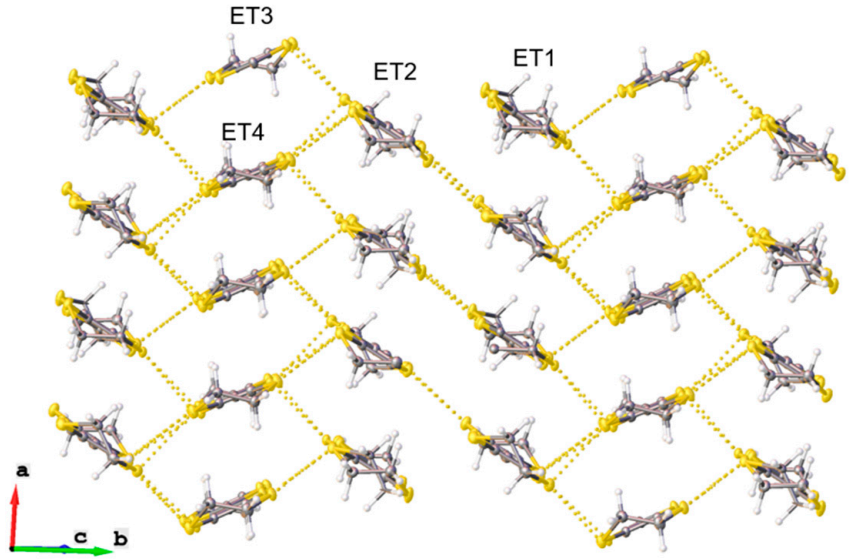


Figure 2. Donor arrangement of **I** on the ab plane. Dashed yellow lines are S···S contacts. ET is an abbreviation for BEDT-TTF.

Cu^{2+} is octahedrally coordinated by six O atoms from three bisbidentate oxalate ligands. The Cu1–O distances are 1.960(4)~2.045(4) Å in the equatorial plane and 2.230(4) Å and 2.362(6) Å from the apex. The Cu2–O distances are 1.969(5)~1.999(5) Å in the equatorial plane and 2.231(4) Å and 2.327(6) Å from the apex. The elongated bonds in the Jahn–Teller distorted octahedron around Cu are highlighted with blue solid lines (Figure 3). Cu1 and Cu2 are adjacent to each other. A honeycomb lattice is formed in the *ab* plane as observed in $[(C_3H_7)_3NH]_2[Cu_2(\mu\text{-}C_2O_4)_3{\cdot}2.2H_2O]$, θ^{21}-$(BEDT\text{-}TTF)_3[Cu_2(\mu\text{-}C_2O_4)_3{\cdot}2CH_3OH]$ and θ^{21}-$(BETS\text{-}TTF)_3[Cu_2(\mu\text{-}C_2O_4)_3{\cdot}2CH_3OH]$ (Figure 3) [43–45]. Solvent molecules occupy the cavities of the honeycomb lattice. The two donor layers are separated by an anion sheet along the *c* axis (Figure 4). Hydrogen bonds exist between the donor and anion, as well as between the anion and solvent molecules (Figure 4).

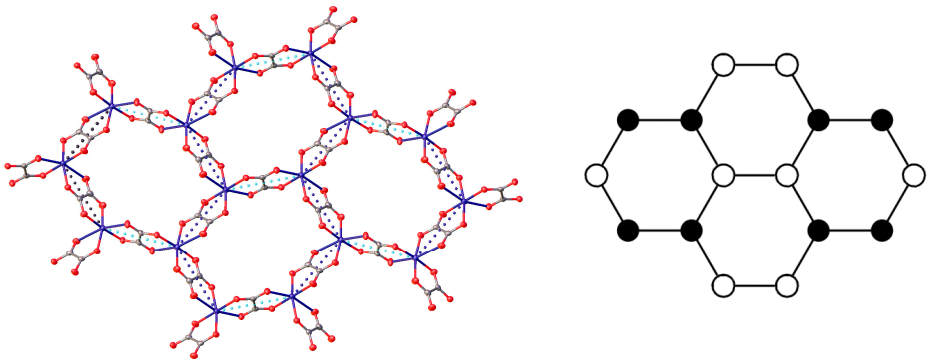


Figure 3. Anion layer of **I** viewed along the *c* axis.

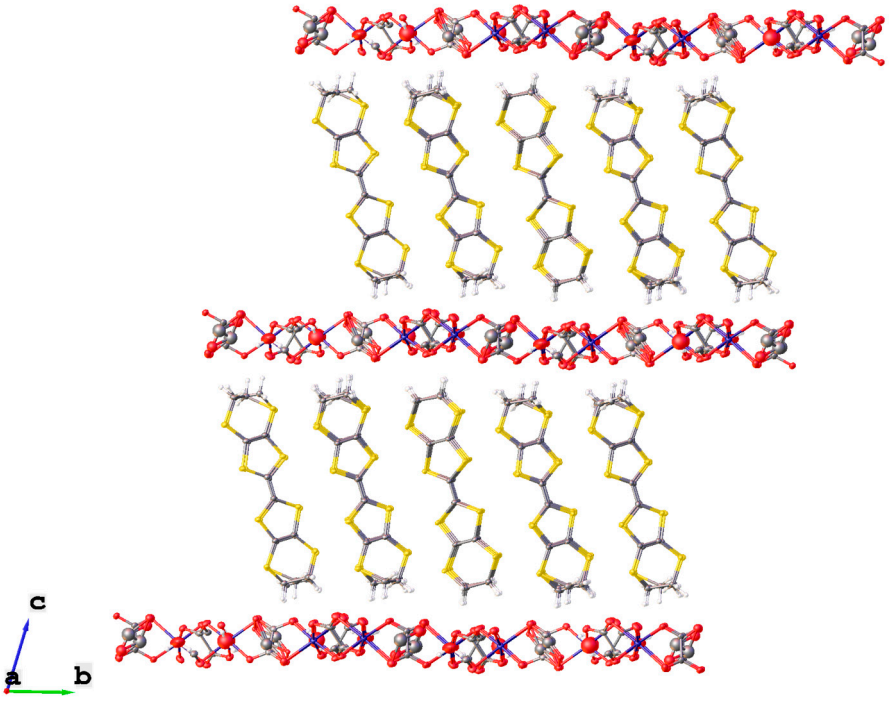
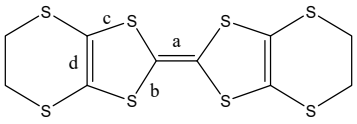


Figure 4. Packing diagram of **I** viewed along the a axis. Color code: Cu, blue; O red: S, yellow; C gray. Hydrogen bond, dashed blue line.

Considering the bond length of a TTF core with a standard deviation of 0.1 of δ, the oxidation state of ET1 is +2/3, while ET2 and ET3 have oxidation states greater than +2/3, and ET4 has an oxidation state less than +1/2. The oxidation states of ET2 and ET3 decreased as the temperature increased. At 290 K, the oxidation states are +0.70 for ET1, +2/3 for ET2, +2/3 for ET3 and +0.43 for ET4. The total oxidation state in an independent unit is +1.98 (Table 1) [50].

The C=C stretching frequency of the charge–transfer complexes of BEDT-TTF serves as a reliable metric for determining the oxidation state of BEDT-TTF [51]. In the Raman spectra (λ = 514.5 nm), a broad band was observed at 1490 cm^{-1} (Figure 5). This corresponds to charge–transfer complexes with $BEDT\text{-}TTF^{+2/3}$ and is similar to the 1493 cm^{-1} band observed for θ^{21}-$(BEDT\text{-}TTF)_3[Cu_2(\mu\text{-}C_2O_4)_3{\cdot}2CH_3OH]$ [44]. The weak band at 1427 cm^{-1} is attributed to ET2, corresponding to an oxidation state ranging from +1/4 to +3/4. It aligns with the formal charge assigned based on the bond lengths in the TTF core.

Table 1. Bond lengths of the TTF core in BEDT-TTF of **I** at 100 K.



			$\delta = (b + c) - (a + d)$			
			$Q = 6.347 - 7.463\delta$			
	a	*b*	*c*	*d*	δ	*Q*
ET1	1.370	1.741 1.740 1.735 1.746	1.748 1.756 1.750 1.758	1.363 1.359	0.763	0.65
	~1.370 *	~1.741	~1.753	~1.361		
ET2	1.379	1.737 1.734 1.733 1.734	1.748 1.746 1.752 1.741	1.362 1.355	0.744	0.80
	~1.370	~1.735	~1.747	~1.359		
ET3	1.382	1.722 1.728	1.744 1.746	1.352	0.736	0.85
	~1.382	~1.725	~1.745	~1.352		
ET4	1.354	1.753 1.756	1.756 1.765	1.337	0.824	0.20
	~1.354	~1.755	~1.761	~1.337		
Total						1.975 **

* The average value of bond lengths. ** Total charge of two and two half donors in an independent unit: $\Sigma Q = Q_{ET1} + Q_{ET2} + 1/2Q_{ET3} + 1/2_{ET4}$.

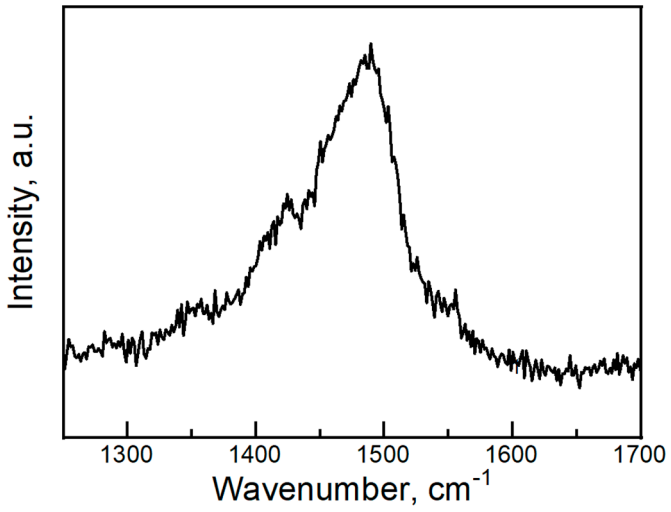


Figure 5. Raman spectrum of **I** with λ = 514.5 nm.

The conductivity measurement was conducted using a four-probe method in a Quantum Design PPMS 9 system. Gold wire was affixed to the best-developed surface of a single crystal with gold paste. The room-temperature conductivity was σ_{rt} = 0.02 S/cm. This value is lower than σ_{rt} = 4 S/cm for θ^{21}-(BEDT-TTF)$_3$[Cu$_2$(μ-C$_2$O$_4$)$_3$·2CH$_3$OH], and significantly lower than σ_{rt} = 140 S/cm for θ^{21}-(BETS-TTF)$_3$[Cu$_2$(μ-C$_2$O$_4$)$_3$·2CH$_3$OH] [44,45]. The conductivity decreased as the temperature dropped, with E_α = 40 meV indicating semiconductor behavior (Figure 6).

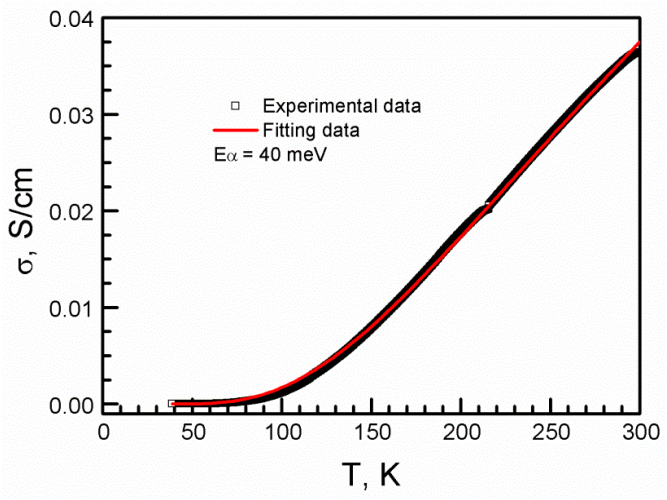


Figure 6. Temperature-dependent conductivity of **I**.

The unpaired electron of Cu(II) is located in the magnetic orbital $d_{x^2-y^2}$ within the equatorial plane. The orbital corresponding to the elongated octahedral Cu(II) is the d_{z^2} orbital, as indicated by the blue solid line highlighted in Figure 3. The magnetic configuration is a stripy antiferromagnetic state [52]. Since the antiferromagnetic interaction is stronger than the ferromagnetic interaction between oxalate-bridged Cu(II) atoms, an antiferromagnetic behavior is expected [12].

The magnetic susceptibility measurement was carried out on Quantum Design MPMS 7XL system. The susceptibility data were corrected by the Pascal constant of the sample and the sample holder [53].

At 300 K, the χT value was 0.389 cm^3 K mol^{-1} and g was 2.04. This is consistent with an isolated, spin only Cu(II) ion with $S = 1/2$ and $g = 2.00$ [54]. As the temperature decreased, the χ increased smoothly, exhibiting a bend around 230 K, followed by an upturn at 22 K. The data fitted to the Curie–Weiss law yielded C = 0.503(2) cm^3 mol^{-1}, $\theta = -87(2)$ K and $R = 9.6 \times 10^{-7}$ above 230 K, while C = 0.405(1) cm^3 mol^{-1}, $\theta = -25.2(7)$ K and $R = 1.3 \times 10^{-5}$ from 100 K to 230 K (Figure 7). No bifurcation is observed from zero-field-cooling magnetization and field-cooling magnetization (ZFCM/FCM) above 2 K under 100 G (Figure 8). No long-range ordering was detected above 2 K. As such, it is a spin-frustrated complex with $f > 12$ [54].

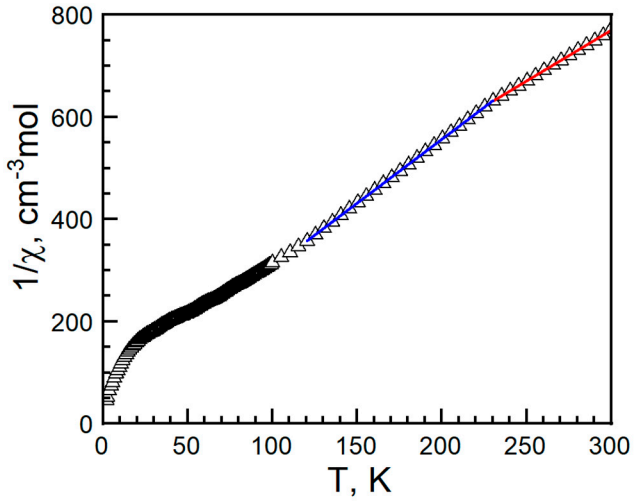


Figure 7. $1/\chi$ vs. T (empty black triangle) of **I**. The red and solid lines are fit to the Curie–Weiss law.

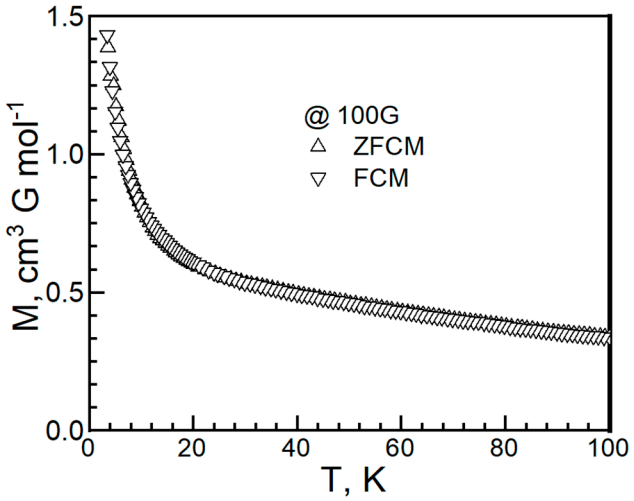


Figure 8. ZFCM/FCM of polycrystal under 100G.

Specific heat measurements were performed from 2 to 120 K under 0 T and 8 T, utilizing a Quantum Design PPMS9 system (Figure 9). No λ-peak was detected in the range of 2 to 120 K. When combined with the X-ray diffraction experiment from 280 K to 120 K, there was no long-range order observed above 2 K.

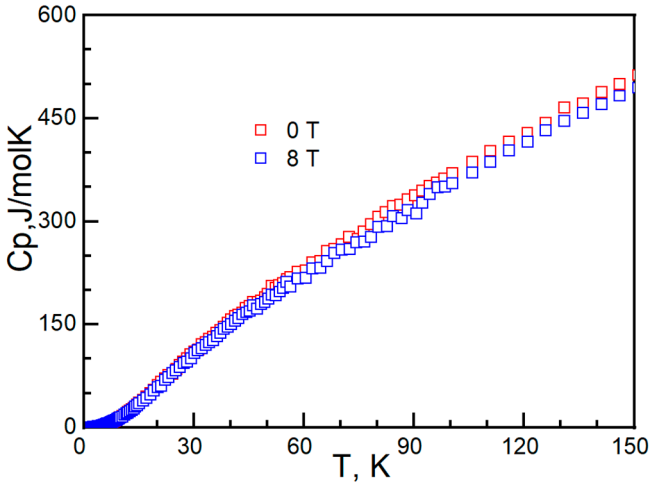


Figure 9. Specific heat of **I** from 2 K to 120 K.

Isothermal magnetization at 2 K increased with the magnetic field, reaching 0.162 N_β at 65 kG (Figure 10). This value surpasses the 0.077 N_β for θ^{21}-(BEDT-TTF)$_3$[Cu_2(μ-C_2O_4)$_3$·2CH_3OH], 0.076 N_β of θ^{21}-(BETS-TTF)$_3$[Cu_2(μ-C_2O_4)$_3$·2CH_3OH] and 0.040 N_β for [(C_3H_7)$_3$NH]$_2$[Cu_2(μ-C_2O_4)$_3$·2.2H_2O] at 2 K and 65 kG [42–44].

Compared with θ^{21}-(BEDT-TTF)$_3$[Cu_2(μ-C_2O_4)$_3$·2CH_3OH] and θ^{21}-(BETS-TTF)$_3$ [Cu_2(μ-C_2O_4)$_3$·2CH_3OH], the conductivity is contributed by the organic donor. The solvent molecule influences the magnetic properties of compounds.

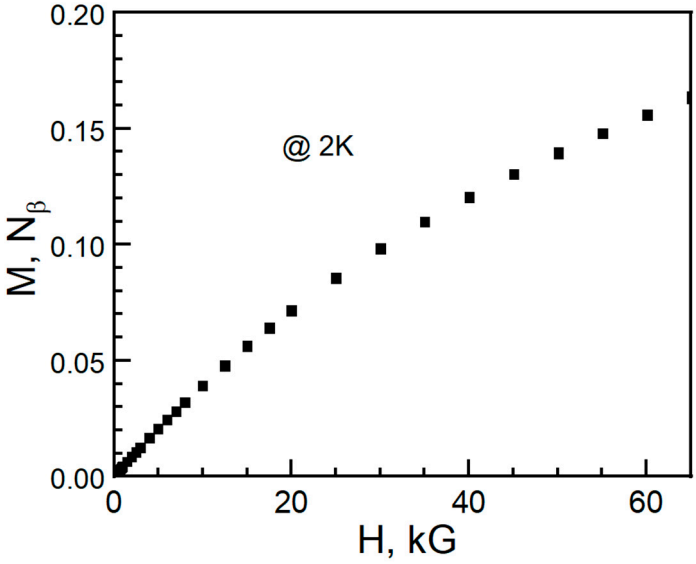


Figure 10. Isothermal magnetization of **I** at 2 K.

3. Conclusions

In this study, we show an organic–inorganic hybrid charge–transfer complex composed of a θ^{21}-phase organic donor layer and an inorganic sheet featuring a honeycomb lattice. The Jahn–Teller effect on the transport and magnetism of organic-inorganic hybrid charge–transfer complexes, influenced by solvent molecules hosted in the honeycomb Cu-oxalate-framework, was studied. It exhibits a semiconducting behavior with E_α = 40 meV. An antiferromagnetic interaction with the spin frustration f > 10 occurs, with no long-range order observed above 2 K. Thus, it is a candidate semiconducting quantum spin liquid.

Supplementary Materials: The following supporting information can be downloaded at: https://www.mdpi.com/article/10.3390/magnetochemistry11020012/s1, Table S1. The crystallographic data of **I** at 290 K, 180 K, 120 K. Table S2. Bond lengths of Cu–O in **I** at 290 K, 180 K and 120 K. Table S3. Bond lengths of the TTF core in BEDT-TTF of **I** at 290 K, 180 K and 120 K. X-ray crystallographic data supplied by CCDC 2417702/2412001/2417459/2417460.

Author Contributions: The manuscript was written with the contributions of all authors. Funding acquisition B.Z.; B.Z. and Y.Z. synthesized the sample.; Y.Z. Performed the transport and magnetic measurements; G.C., Z.G., Z.W., T.L. and Y.S. performed the X-ray experiments and data analysis: D.W. performed specific heat experiment and data analysis; Y.G. performed Raman experiment and data validation; F.L., Z.Z., X.Z. (Xiaoyu Zhang), B.Q., P.X. and J.W. performed the XPS experiments and data validation, F.D. performed thin film of crystal, D.Y. performed the EDS experiment, Q.L. and X.L., performed element anlysis and R.F. performed IR spectra measuremetn. M.L. and X.Z. (Xueying Zhang) performed data valiation, B.Z., Y.Z. and Z.W. analyzed all of the data. B.Z., Y.Z. and Z.W. wrote the main manuscript text. All authors have read and agreed to the published version of the manuscript.

Funding: This research was funded by the National Natural Science Foundation of China: 22273109, 22073106, 21573242 and 21173230.

Institutional Review Board Statement: Not applicable.

Informed Consent Statement: Not applicable.

Data Availability Statement: CCDC 2417702/2412001/2417459/2417460 contain the supplementary crystallographic data for compounds **I** at 100 K, 120 K, 180 K and 290 K, respectively. These data can be obtained free of charge via https://www.ccdc.cam.ac.uk/structures/ (accessed on 21 January 2025) or from Cambridge Crystallographic Data Centre, 12 Union Road, Cambridge CB2 1EZ, UK;

fax: (+44) 1223-336-033; or e-mail: deposit@ccdc.cam.ac.uk. The original contributions presented in this study are included in the article/Supplementary Material. Further inquiries can be directed to the corresponding authors.

Conflicts of Interest: The authors declare no conflicts of interest.

References

1. Anderson, P.W. Resonating Valence Bonds: A New Kind of Insulator. *Mater. Res. Bull.* **1973**, *8*, 153–160. [CrossRef]
2. Bednorz, J.G.; Muller, K.A. Possible High T_c Superconductivity in the Ba−La−Cu−O System. *Z. Phys. B. Condensed Matter* **1986**, *64*, 189–193. [CrossRef]
3. Anderson, P.W. The Resonating Valence Bond State in La_2CuO_4 and Superconductivity. *Science* **1987**, *235*, 1197–1198. [CrossRef] [PubMed]
4. Balents, L. Spin liquids in frustrated magnets. *Nature* **2010**, *464*, 199–208. [CrossRef] [PubMed]
5. Broholm, C.; Cava, R.J.; Kivelson, S.A.; Nocera, D.G.; Norman, M.R.; Senthil, T. Quantum Spin Liquids. *Science* **2020**, *367*, eaay0668. [CrossRef] [PubMed]
6. Williams, J.M.; Schultz, A.J.; Geiser, U.; Carlson, K.D.; Kini, A.M.; Wang, H.H.; Kwok, W.; Whangbo, M. Organic Superconductors—New Benchmarks. *Science* **1991**, *252*, 1501–1508. [CrossRef] [PubMed]
7. Pratt, F.L.; Baker, P.J.; Blundell, S.J.; Lancaster, T.; Ohira-Kawamura, S.; Baines, C.; Shimizu, Y.; Kanoda, K.; Watanabe, I.; Saito, G. Magnetic and non-magnetic phase of quantum spin liquid. *Nature* **2011**, *471*, 612–616. [CrossRef]
8. Shimizu, Y.; Hiramatsu, T.; Maesato, M.; Otsuka, A.; Yamochi, H.; Ono, A.; Itoh, M.; Yoshida, M.; Takigawa, M.; Yoshida, Y.; et al. Pressure-Tuned Exchange Coupling of q Quan Spin Liquid in the Molecular Triangular Lattice κ-$(ET)_2Ag_2(CN)_3$. *Phys. Rev. Lett.* **2016**, *117*, 107203. [CrossRef] [PubMed]
9. Yamashita, M.; Nakata, N.; Senshu, Y.; Nagata, M.; Yamamoto, H.M.; Kato, R.; Shibauchi, T.; Matsuda, Y. Highly Mobile Gapless Excitations in a Two-Dimensional Candidate Quantum Spin Liquid. *Science* **2010**, *328*, 1246–1268. [CrossRef]
10. Isono, T.; Kamo, H.; Ueda, A.; Takahashi, K.; Kimata, M.; Tajima, H.; Tsuchiya, S.; Terashima, T.; Uji, S.; Mori, H. Gapless Quantum Spin Liquid in an Organic Spin-1/2 Triangular-Lattice κ-H_3(cat-EDT-TTF)$_2$. *Phys. Rev. Lett.* **2014**, *112*, 177201. [CrossRef] [PubMed]
11. Baudron, S.A.; Batail, P.; Coulon, C.; Clérac, R.; Canadell, E.; Laukhin, V.; Melzi, R.; Wzietek, P.; Jérome, D.; Auban-Senzier, P.; et al. (EDT-TTF-$CONH_2)_6[Re_6Se_8(CN)_6]$, a Metallic Kagome-Type Organic−Inorganic Hybrid Compound: Electronic Instability, Molecular Motion, and Charge Localization. *J. Am. Chem. Soc.* **2005**, *127*, 11785–11797. [CrossRef]
12. Cano, J.; Alemany, P.; Alvarez, S.; Verdaguer, M.; Ruiz, E. Exchange Coupling in Oxalato-Bridged Copper(II) Binuclear Compounds: A Density Functional Study. *Chem. Eur. J.* **1998**, *4*, 476–484. [CrossRef]
13. Hursthouse, M.B.; Light, M.E.; Price, D.J. One-dimensional Magnetism in Anhydrous Iron and Cobalt Ternary Oxalates with Rare Trigonal-Prismatic Metal Coordination Environment. *Angew. Chem. Int. Ed.* **2004**, *43*, 472–475. [CrossRef]
14. Xu, H.; Wang, Z.; Liu, T.; Gao, S. Synthesis, Structure, and Magnetic Properties of (A)[Fe^{III}(oxalate)Cl_2] (A = Alkyl Ammonium Cations) with Anionic 1D [Fe^{III}(oxalate)$Cl_2]^-$ Chains. *Inorg. Chem.* **2007**, *46*, 3089–3096. [CrossRef] [PubMed]
15. Duan, Z.; Zhang, Y.; Zhang, B.; Zhu, D. $Co(C_2O_4)(HO(CH_2)_3OH)$: An Antiferromagnetic Neutral Zigzag Chain Compound Showing Long-Range Ordering of Spin Canting. *Inorg. Chem.* **2008**, *47*, 9152–9154. [CrossRef] [PubMed]
16. Zhang, B.; Zhang, Y.; Chang, G.; Wang, Z.; Zhu, D. Crystal-to-Crystal Transformation from $K_2[Co(C_2O_4)_2(H_2O)_2]\cdot 4H_2O$ to $K_2[Co(\mu\text{-}C_2O_4)(C_2O_4)]$. *Magnetochemistry* **2021**, *7*, 77. [CrossRef]
17. Mathoniere, C.; Nuttall, C.J.; Carling, G.; Day, P. Ferrimagnetic Mixed-Valency and Mixed-Metal Tris(oxalato)iron(III) Compounds: Synthesis, Structure, and Magnetism. *Inorg. Chem.* **1996**, *35*, 1201–1206. [CrossRef]
18. Tamaki, H.; Zhong, Z.J.; Matsumoto, N.; Kida, S.; Koikawa, M.; Achiwa, N.; Hashimoto, Y.; Okawa, H. Design of Metal-Complex Magnets. Syntheses and Magnetic Properties of Mixed-Metal Assemblies $\{NBu_4[MCr(ox)_3]\}$ (NBu_4^+ = Tetra(n-buty1)ammonium Ion; ox^{2-} = Oxalate Ion; M = Mn^{2+}, Fe^{2+}, Co^{2+}, Ni^{2+}, Cu^{2+}, Zn^{2+}). *J. Am. Chem. Soc.* **1992**, *114*, 6974–6979. [CrossRef]
19. Zhang, B.; Zhang, Y.; Zhang, J.; Li, J.; Zhu, D. A neutral molecular-based layered magnet $[Fe(C_2O_4)(CH_3OH)]_n$ exhibiting magnetic ordering at $T_N \approx 23$ K. *Dalton Trans.* **2008**, 5037–5040. [CrossRef]
20. Rousse, G.; Rodriguez-Carvajal, J. Oxalate-mediated long-range antiferromagnetism order in $Fe_2(C_2O_4)_3\cdot 4H_2O$. *Dalton Trans.* **2016**, *45*, 14311–14319. [CrossRef] [PubMed]
21. Decurtins, S.; Schmalle, H.W.; Schneuwly, P.; Ensling, J.; Gutlich, P. A Concept for the Synthesis of 3-Dimensional Homo- and Bimetallic Oxalate-Bridged Networks $[M_2(ox)_3]_n$. Structural, Mössbauer, and Magnetic Studies in the Field of Molecular-Based Magnets. *J. Am. Chem. Soc.* **1994**, *116*, 9521–9528. [CrossRef]
22. Hernandez-Molina, M.; Lloret, F.; Ruiz-Perez, C.; Julve, M. Weak Ferromagnetism in Chiral 3-Dimensional Oxalato-Bridged Cobalt(II) Compounds. Crystal Structure of $Co(bpy)_3][Co_2(ox)_3]ClO_4$. *Inorg. Chem.* **1998**, *37*, 4131–4145. [CrossRef]

23. Coronado, E.; Galan-Mascaros, J.R.; Gomez-Garzia, C.J.; Martinez-Agudo, J.M. Molecule-Based Magnets Formed by Bimetallic Three-Dimensional Oxalate Networks and Chiral Tris(bipyridyl) Complex Cations. The Series Tris(bipyridyl) Complex Cations. The Series $[Z^{II}(bpy)_3][ClO_4][M^{II}Cr^{III}(ox)_3]$ (Z^{II} = Ru, Fe, Co, and Ni; M^{II} = Mn, Fe, Co, Ni, Cu, and Zn; ox = Oxalate Dianion). *Inorg. Chem.* **2001**, *40*, 113–120.
24. Mon, M.; Grancha, T.; Verdaguer, M.; Train, C.; Armentano, D.; Pardo, E. Solvent-Dependent Self-Assembly of an Oxalato-Based ThreeDimensional Magnet Exhibiting a Novel Architecture. *Inorg. Chem.* **2016**, *55*, 6845–6847. [CrossRef] [PubMed]
25. Zhang, B.; Zhang, Y.; Zhang, J.; Xiang, H.; Zhu, D. $Mn(C_2O_4)(H_2O)_{0.25}$: An antiferromagnetic oxalato-based cage compound. *Dalton Trans.* **2011**, *40*, 5430–5432. [CrossRef] [PubMed]
26. Coronado, E.; Galan-Mascaros, J.R.; Marti-Gastaldo, C. Single chain magnets based on the oxalate ligand. *J. Am. Chem. Soc.* **2008**, *130*, 14987–14989. [CrossRef]
27. Thomas, T.W.; Che-Hsiung, H.; Labes, M.M.; Gomm, P.S.; Underhill, A.E.; Watkins, D.M. Temperature Dependence of Conductivity of Some Partly-Oxidised Platinum Complexes. *J. Chem. Soc. Dalton* **1972**, 2050–2053. [CrossRef]
28. Braude, A.; Carneiro, K.; Jacobsen, C.S.; Mortensen, K.; Turner, D.J.; Underhill, A.E. Solid-state properties of one-dimensional metals based on bis(oxalate)platinate anions with divalent cations. *Phys. Rev. B* **1987**, *36*, 7835–7846. [CrossRef] [PubMed]
29. Gartner, S.; Heinen, I.; Schveitzer, D.; Nuber, B.; Keller, H.J. BEDT-TTF salts with square platinates (II) as counterions: $(BEDT\text{-}TTF)_4[Pt(C_2O_4)_2]$. A new organic metal. *Synth. Met.* **1989**, *31*, 199–213. [CrossRef]
30. Wang, X.; Ge, C.; Xing, X.; Wang, P.; Zhang, D.; Wu, P.; Zhu, D. Preparation and properties of a new organic conductor $(BEDT\text{-}TTF)_4Cu(C_2O_4)_2$. *Synth. Met.* **1991**, *39*, 355–358. [CrossRef]
31. Wang, P.; Bandow, S.; Maruyama, Y.; Wang, X.; Zhu, D. Physical and structure properties of a new organic conductor $(BEDT\text{-}TTF)_4Cu(C_2O_4)_2$. *Synth. Met.* **1991**, *44*, 147–157. [CrossRef]
32. Kurmoo, M.; Graham, A.W.; Day, D.; Simon, J.C.; Hursthouse, M.B.; Caufield, J.L.; Singleton, J.; Pratt, F.L.; Hayes, W.; Ducasse, L.; et al. Superconducting and Semiconducting Magnetic Charge Transfer Salts: $(BEDT\text{-}TTF)_4AFe(C_2O_4)_3{\cdot}C_6H_5CN$. *J. Am. Chem. Soc.* **1995**, *117*, 12209–12217. [CrossRef]
33. Cassoux, P. A Molecular Paramagnetic Superconductor. *Science* **1996**, *272*, 1277–1278. [CrossRef]
34. Zhang, B.; Wang, Z.; Fujiwara, H.; Kobayashi, H.; Kurmoo, M.; Inoue, K.; Mori, T.; Gao, S.; Zhang, Y.; Zhu, D. Tetrathiafulvalene $[Fe^{III}(C_2O_4)Cl_2]$: An organic-inorganic hybrid exhibiting canted antiferromagnetism. *Adv. Mater.* **2005**, *17*, 1988–1991. [CrossRef]
35. Zhang, B.; Wang, Z.; Zhang, Y.; Takahashi, K.; Okano, Y.; Cui, H.; Kobayashi, H.; Inoue, K.; Kurmoo, M.; Pratt, F.; et al. Hybrid organic-inorganic conductor with a magnetic chain anion: κ-$BETS_2[Fe^{III}(C_2O_4)Cl_2]$ [BETS = bis(ethylenedithio)tetraselenafulvalene]. *Inorg. Chem.* **2006**, *45*, 3275–3280. [CrossRef]
36. Zhang, B.; Zhang, Y.; Gao, Z.; Chang, G.; Su, S.; Wang, D.; Guo, Y.; Zhu, D. Synthesis, Crystal Structure, and Characterization of the Charge-transfer Salt: $(BEDT\text{-}TTF)[Fe(C_2O_4)Cl_2](CH_2Cl_2)$, (BEDT-TTF = bis(ethylenedithio)tetrathiafulvalene). *Eur. J. Inorg. Chem.* **2014**, *2014*, 4028–4032. [CrossRef]
37. Zhang, B.; Zhang, Y.; Wang, Z.; Yang, D.; Gao, Z.; Wang, D.; Guo, Y.; Zhu, D.; Mori, T. $[BEDT\text{-}TTF][Fe(C_2O_4)Cl_2]$: An organic–inorganic hybrid semiconductive antiferromagnet. *Dalton Trans.* **2016**, *45*, 16561–16565. [CrossRef] [PubMed]
38. Palacio, F.; Miller, J.S. A dual-function material. *Nature* **2000**, *408*, 421–422. [CrossRef] [PubMed]
39. Coronado, E.; Galan-Mascaros, J.R.; Gomez-Garcia, C.J.; Laukin, V. Coexistence of ferromagnetism and metallic conductivity in a molecular-based layered compound. *Nature* **2000**, *408*, 447–449. [CrossRef] [PubMed]
40. Alberola, A.; Coronado, E.; Galan-Mascaros, J.R.; Gimenez-Saiz, C.; Gimene-Garcia, C.J. A Molecular Metal Ferromagnet from the Organic Donor Bis(ethylenedithio)tetraselenafulvalene and Bimetallic Oxalate Complexes. *J. Am. Chem. Soc.* **2003**, *125*, 10774–10775. [CrossRef] [PubMed]
41. Jahn, H.A.; Teller, E. Stability of polyatomic molecules in degenerate electronic states-I—Orbital degeneracy. *Proc. R. Soc. Lond. Ser. A Math. Phys. Sci.* **1937**, *161*, 220–235.
42. Zhang, B.; Zhang, Y.; Wang, Z.; Sun, Y.; Liang, T.; Liu, M.; Zhu, D. Two One-dimensional Copper-Oxalate Frameworks with the Jahn–Teller Effect: $[(CH_3)_3NH]_2[Cu(\mu\text{-}C_2O_4)(C_2O_4]{\cdot}2.5H_2O$ (I) and $[(C_2H_5)_3NH]_2[Cu(\mu\text{-}C_2O_4)(C_2O_4)]{\cdot}H_2O$. *Magnetochemistry* **2023**, *9*, 120. [CrossRef]
43. Zhang, B.; Zhang, Y.; Wang, Z.; Wang, D.; Baker, P.; Pratt, F.; Zhu, D. Candidate Quantum Spin Liquid due to Dimensional Reduction of a Two-Dimensional Honeycomb Lattice. *Sci. Rep.* **2014**, *4*, 6451. [CrossRef] [PubMed]
44. Zhang, B.; Zhang, Y.; Zhu, D. $(BEDT\text{-}TTF)_3[Cu_2(C_2O_4)_3](CH_3OH)_2$: An organic-inorganic hybrid antiferromagnetic semiconductor. *Chem. Commun.* **2012**, *48*, 197–199. [CrossRef] [PubMed]
45. Zhang, B.; Zhang, Y.; Wang, Z.; Gao, S.; Guo, Y.; Liu, F.; Zhu, D. $BETS_3[Cu_2(C_2O_4)_3](CH_3OH)_2$: An organic–inorganic hybrid antiferromagnetic metal (BETS = bisethylene(tetraselenfulvalene)). *CrystEngComm* **2013**, *15*, 3529–3535. [CrossRef]
46. Zhang, B.; Zhang, Y.; Zhu, D. $[(C_2H_5)_3NH]_2Cu_2(C_2O_4)_3$: A three-dimensional metal-oxalato framework showing structurally related dielectric and magnetic transitions at around 165 K. *Dalton Trans.* **2012**, *14*, 8509–8511. [CrossRef] [PubMed]
47. Zhang, B.; Baker, P.; Zhang, Y.; Wang, D.; Wang, Z.; Su, S.; Zhu, D. Quantum Spin Liquid from a Three-Dimensional Copper-Oxalate Framework. *J. Am. Chem. Soc.* **2018**, *140*, 122–125. [CrossRef]

48. Geim, A.K.; Novoselov, K.S. The rise of graphene. *Nat. Mater.* **2007**, *6*, 183–191. [CrossRef] [PubMed]
49. Sheldrick, G.M. *SHELXL-2012/7*, University of Göttingen: Göttingen, Germany, 2014.
50. Guionneau, P.; Kepert, C.J.; Bravic, G.; Chasseau, D.; Truter, M.R.; Kurmoo, M.; Day, P. Determing the charge distribution in BEDT-TTD salts. *Synth. Met.* **1997**, *86*, 1973–1974. [CrossRef]
51. Wang, H.H.; Ferraro, J.R.; Williams, J.M.; Geiser, U.; Schlueter, J.A. Rapid Raman Spectroscopic Determination of the Stoichiometry of Microscopic Quantities of BEDT-TTF-based Organic Conductors and Superconductors. *J. Chem. Soc. Chem. Commun.* **1994**, 1893–1894. [CrossRef]
52. Price, C.C.; Perkins, N.B. Critical Properties of the Kitaev-Heisenberg Model. *Phy. Rev. Lett.* **2012**, *109*, 187201. [CrossRef]
53. Kahn, O. *Molecular Magnetism*; John Wiley & Sons Inc.: New York, NY, USA, 1993.
54. Ramirez, A.P. Strongly geometrically frustrated magnets. *Annu. Rev. Mater. Sci.* **1994**, *24*, 453–480. [CrossRef]

Disclaimer/Publisher's Note: The statements, opinions and data contained in all publications are solely those of the individual author(s) and contributor(s) and not of MDPI and/or the editor(s). MDPI and/or the editor(s) disclaim responsibility for any injury to people or property resulting from any ideas, methods, instructions or products referred to in the content.